2009-2012 DOE FINAL TECHNICAL REPORT

Molecular-level Design of Heterogeneous Chiral Catalysts
DE-SC0002448

PI's: Andrew J. Gellman (Carnegie Mellon University, gellman@cmu.edu)
Davis S. Sholl (Georgia Tech, david.sholl@chbe.gatech.edu)
Wilfred T. Tysoe (U. of Wisconsin – Madison, wtt@uwm.edu)
Francisco Zaera (U. of California – Riverside, zaera@ucr.edu)

Personnel: Luke Burkholder (Post-doctoral researcher)
Yun Bai (Post-doctoral Researcher)
Ilkeun Lee (Post-doctoral Researcher)
Anibal Boscoboinik (Graduate Student, Graduated 2011)
Xin Yang (Graduate Student, Graduated 2011)
Xiao Xiao (Graduate Student, Graduated 2011)
Junghyun Hong (Visiting Scholar)
Brian Holsclaw (Graduate Student, Graduated 2012)
Mausumi Mahapatra (Graduate Student)
Bharat Mahtre (Graduate Student)
Yongju Yun (Graduate Student)
Vladimir Pushkarev (Grad Student, Graduated 2010)
Wai-Yeng Cheong (Grad Student, Graduated 2010)

Collaborators:

Prof. Giorgio Zgrablich (National University of San Luis, Argentina)
Michael Weinert (Department of Physics, UW-Milwaukee)
Nisha Shukla (Institute for Complex Engineered Systems, Carnegie Mellon University)

Annual Budget: $660,000

Execution Period: 09/15/2009 – 09/14/2012

A. Abstract – Summary of significant results

Understanding and controlling selectivity is one of the key challenges in heterogeneous catalysis. Among problems in catalytic selectivity enantioselectivity is perhaps the most the most challenging. The primary goal of the project on "Molecular-level Design of Heterogeneous Chiral Catalysts" is to understand the origins of enantioselectivity on chiral heterogeneous surfaces and catalysts. The efforts of the project team include preparation of chiral surfaces, characterization of chiral surfaces, experimental detection of enantioselectivity on such surfaces and computational modeling of the interactions of chiral probe molecules with chiral surfaces. Over the course of the project period the team of PI's has made some of the most detailed and insightful studies of enantioselective chemistry on chiral surfaces. This includes the measurement of fundamental interactions and reaction mechanisms of chiral molecules on chiral surfaces and leads all the way to rationale design and synthesis of chiral surfaces and materials for enantioselective surface chemistry. The PI's have designed and prepared new materials for enantioselective adsorption and catalysis.

Naturally Chiral Surfaces

- Completion of a systematic study of the enantiospecific desorption kinetics of R-3-methylcyclohexanone (R-3-MCHO) on 9 achiral and 7 enantiomeric pairs of chiral Cu surfaces with orientations that span the stereographic triangle.
- Discovery of super-enantioselective tartaric acid (TA) and aspartic acid (Asp) decomposition as a result of a surface explosion mechanism on Cu(643)$^{R\&S}$. Systematic study of super-enantiospecific TA and Asp decomposition on five enantiomeric pairs of chiral Cu surfaces.
- Initial observation of the enantiospecific desorption of R- and S-propylene oxide (PO) from Cu(100) imprinted with {3,1,17} facets by L-lysine adsorption.

Templated Chiral Surfaces

- Initial observation of the enantiospecific desorption of R- and S-PO from Pt(111) and Pd(111) modified by a variety of chiral templates.
- Demonstrated enantioselective separation of racemic PO on chemically synthesized chiral gold nanoparticles.
- Discovery of zwitterionic adsorption states of amino acids on Pd(111).
- First structure determinations of adsorbed amino acids and identification of tetrameric chiral template structures.
- Exploration of the enantiospecific interaction of PO and R-3-MCHO adsorption on chirally modified Cu(100), Cu(110) and Cu(111).

One-to-One Interactions

- Determination of cinchona orientation on Pt surfaces in situ at the solid-liquid interface using FT-IRAS.
- Systematic study of the influence of solution properties on the adsorption of modified cinchonas alkaloids onto Pt surfaces.
- Correlation of cinchona adsorption with catalytic activity, as affected by concentration, the nature of the solvent, and dissolved gases in the liquid phase.

- Measurement of enantioselective chemisorption on 1-(1-naphthyl) ethylamine (NEA) modified Pt(111) and Pd(111) surfaces.
- Imaging of chiral docking complexes between NEA and methyl pyruvate on Pd(111).

Chiral Catalyst Synthesis

- Anchoring of cinchona alkaloid to surfaces
- Synthesis of chiral Au nanoparticles and demonstration of their enantiospecific interactions with R- and S-PO.
- Elucidation of the driving forces for chiral imprinting of Cu(100) by L- and D-lysine to form Cu(3,1,17)$^{R\&S}$ facets.

B. Accomplishments

B.1. Scope and goals of program

The scope of the project on "Molecular-level Design of Heterogeneous Chiral Catalysts" is divided into three areas defined by the three types of chiral surfaces identified by the PIs: naturally chiral surfaces; templated chiral surfaces and surfaces with one-to-one modifiers. Naturally chiral surfaces are low symmetry crystal planes of inorganic materials; metals in this instance. The templated surfaces are surfaces that are modified with adsorbates forming chiral structures with long range. The one-to-one modifiers are molecules that are chiral when adsorbed and induce enantioselectivity through their interactions with other adsorbates.

The efforts to study each of the three types of chiral surfaces include experiment, theoretical modeling, surface preparation, surface characterization and study of enantiospecific interactions with chiral probe compounds. The goals have been:

- to identify and prepare chiral surfaces,
- to identify enantiospecific surface processes involving chiral molecular probes,
- and to characterize these processes to determine the origins of enantioselectivity.

B.2. Accomplishments - Naturally Chiral Surfaces

R-3-methlycyclohexanone on Cu(*hkl*)$^{R\&S}$

Gellman has shown that in TPD experiments the desorption of R-3MCHO from naturally chiral Cu surfaces exhibits features associated with terraces (230 – 260 K), close-packed steps (320 – 340 K) and kinks (350 – 385 K).[1-3] On different chiral Cu surfaces, desorption from chiral kinks is enantiospecific; the peak desorption temperatures from R- and S- kinks differ by 2.0 – 3.5 K, corresponding to an enantiospecific desorption energy differences of 0.6 – 1.0 kJ/mole. Gellman has completed a comprehensive study of the enantiospecific desorption of R-3MCHO from a set of 9 achiral and 7 enantiomeric pairs of chiral Cu single crystal surfaces. Figure 1 shows the ideal structures of

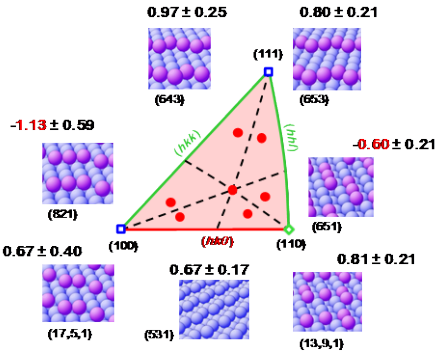

Figure 1. The seven enantiomeric pairs of chiral copper surfaces and the enantiospecificity of the desorption energies of R-3MCHO from these surfaces (kJ/mole).

chiral surfaces around the stereographic triangle and the enantiospecificity of the R-3MCHO desorption energies on each, $\Delta\Delta E_{des}^{S/R} = \Delta E_{des}^{S} - \Delta E_{des}^{R}$. The key point is that, although the magnitude of these desorption energies is always ~1 kJ/mole, they do depend on surface structure; note that the sign of $\Delta\Delta E_{des}^{S/R}$ differs among the surfaces.

PAX Measurements of chiral kink densities on Cu(643)$^{R\&S}$

As indicated earlier, the real structures of the naturally chiral surfaces differ from the ideal ones because thermal roughening by diffusion of atoms along step edges causes the kinks to coalesce. The details of this process were originally modeled on chiral Pt and Cu surfaces by Sholl who showed that although the kink densities are reduced by thermal roughening, the net chirality of the surface is preserved.[4,5] Recently, Gellman has used photoemission of adsorbed Xe (PAX) in conjunction with STM imaging to measure the distribution of terrace-, step- and kink-sites.[5,6] The binding energy of the adsorbed Xe $5p_{1/2}$ photoemission feature depends on the local work function and thus, the local structure of the adsorption site. High-resolution UV photoemission spectra of Xe on the Cu(111), Cu(221) and Cu(643) and on the Pt(111), Pt(221) and Pt(531) surfaces reveal this site sensitivity and have been used to estimate the real site densities on these surfaces.

Super-enantiospecific decomposition - TA and Asp on Cu(*hkl*)$^{R\&S}$

The small enantiospecific energy differences (~1 kJ/mole) between chiral species control enantioselectivity. For a first-order process such as the desorption of R-3MCHO from chiral Cu(*hkl*)$^{R\&S}$ surfaces, such differences lead to differences in desorption rates of ~30% at room temperature. Extremely high enantioselectivities can only be observed for processes that have highly enantiospecific energetics (easy to envision but difficult to achieve), or for processes that have highly non-linear reaction kinetics. Gellman has discovered a type of surface process that is super-enantiospecific; the explosive decomposition of tartaric acid (TA) on naturally chiral Cu surfaces.[7]

During heating, tartaric acid (HO_2C-CH(OH)-CH(OH)-CO_2H) decomposition on Cu occurs by a process that requires an empty site and thus, proceeds with a non-linear rate law of the general form $r = k \cdot \theta(1-\theta)$. When $\theta = 1$, the process must be initiated by a nucleation step that creates empty sites. The decomposition of TA then creates additional empty sites in an autocatalytic process with explosive kinetics. This phenomenology is illustrated beautifully by the isothermal decomposition of L-TA on Cu(651)^{S} (Figure 2). The L-TA-saturated surface was held at T = 450 – 470 K while the rate of CO_2 desorption was monitored mass spectrometrically. At 450 K, there is a 400 sec induction period during which nothing (observable) occurs, and then a relatively short (50 sec) burst of CO_2 desorption as the L-TA decomposition reaction is triggered and proceeds to completion. The inset to Figure 2 illustrates the extremely high enantiospecificity of this autocatalytic reaction. By

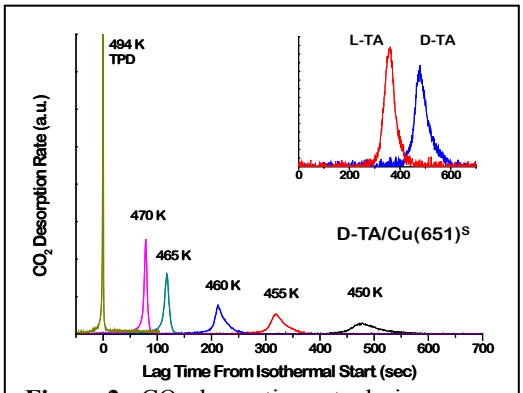

Figure 2. CO_2 desorption rate during isothermal heating of *D*-TA on Cu(651)^{S} at temperature in the range 450 – 470 K. At 0 sec is the TPD peak obtained during heating at 1 K/s. The inset shows the difference in the decomposition rates for *D*- and *L*-TA on Cu(651)^{S}.

the time that the decomposition of L-TA reaches completion on Cu(651)^S, the onset of D-TA decomposition has barely begun; this is a direct consequence of the non-linear kinetics of this process. Simple fitting of these data and the associated TPD spectra suggests that the process is best described by a rate law of the form $r = k_n\theta + k_d \cdot \theta(1-\theta)^2$, where k_n describes a slow nucleation process that creates empty sites and k_d describes the autocatalytic decomposition. Once the empty sites reach a critical coverage, $\theta_c = \sqrt{1-k_n/k_d}$, the autocatalytic reaction dominates and, because of its explosive nature, proceeds to completion in a relatively short time, resulting in the very high enantioselectivity.

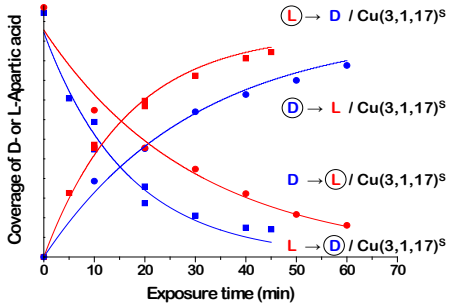

Figure 3. Coverages of *D*- (blue) and *L*- (red) aspartic acid during displacements of *D*- by *L*- (fast) and *L*- by *D*- (slow) on Cu(3,1,17)^S at 460 K.

Enantiospecific isotopomer displacement to probe chiral adsorption

Gellman has also shown that aspartic acid, (Asp, $HO_2CCH(NH_2)$-CH_2-CO_2H), the amino acid analog of tartaric acid, undergoes explosive decomposition on Cu surfaces. The major products are CO_2 and CH_3-C≡N, similar to those found for other amino acids on Pd(111).[8-10] The fact that this occurs for an amino acid opens a world of experimental opportunities for studying super-enantiospecificity because there are 16 different isotopomers of L-aspartic acid available. Isotopomers such as $HO_2{}^{13}C$-$CH(NH_2)$-CH_2-$^{13}CO_2H$ have been used to demonstrate unequivocally that the CO_2 originates solely from the carboxylate end groups.

The critical opportunity created by the availability of isotopically labeled amino acids is the ability to use mass spectrometry to distinguish between enantiomers desorbing from the surface. For example, by exposing a racemic mixture containing equal parts L-aspartic-1,4-$^{13}C_2$ acid and D-aspartic acid to the Cu(3,1,17)^R surface and then using TPD to measure the yields of CO_2 and $^{13}CO_2$ (at q/m = 44 and 45 amu, respectively), the relative coverages of the two enantiomers (isotopomers) has been determined. Although the Cu(3,1,17)^R surface is exposed to a racemic mixture, the adsorbed layer is enantiomerically enriched because one of the two enantiomers adsorbs preferentially. During extended exposures the preferred enantiomer displaces the other until equilibrium is established between the racemic gas phase and an enantiomerically enriched adsorbed phase (Figure 3). Using this method, Gellman has shown that L-Aspartic acid is preferentially adsorbed on the Cu(3,1,17)^S surface (and that D-aspartic acid is preferentially adsorbed on Cu(3,1,17)^R).

B.3. Accomplishments - Templated Chiral Surfaces

Template formation by amino acids

Prior to examining enantioselective adsorption on amino-acid modified surfaces, the surface chemistry of glycine, L-alanine and L-proline were explored on Pd(111) by Tysoe. They are thermally stable to ~350 K, and adsorb in both their anionic and zwitterionic forms. The amino acids thermally decompose at T > 350 K by cleavage of the C-CO_2 bond to evolve an alkyl amine and CO_2.

Enantioselective adsorption was studied on a number of amino acid modified surfaces by measuring differences in the saturation R- and S-PO coverage. It was found that amino acids

with *n*-alkyl side chains (alanine, 2-aminobutanoic acid and norvaline) show enantioselectivity, while those with branched chains (valine, leucine) do not. The conformation of the adsorbed amino acid (zwitterionic or anionic) does not correlate with its enantioselectivity. These experiments were supplemented by DFT calculations by Sholl that showed that the amino acids adsorb to the surface via the carboxylate and amine or amide group.

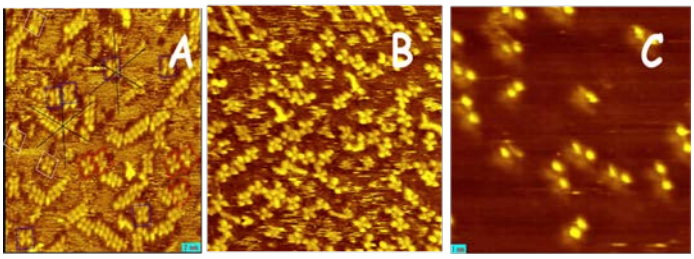

Figure 4. STM images of (A) alanine tetramers, (B) 2-aminobutanoic acid tetramers and (C) valine dimers (non-enantioselective to PO adsorption) on Pd(111).

Since the amino acid conformation does not influence enantioselectivity, we have used STM to examine the distribution of amino acids on a Pd(111) surface. Tetramers of amino acids form on surfaces that show enantioselectivity, while dimers form on surfaces that do not. This strongly suggests that amino acids form surface templates that consist of amino acid tetramers, a hypothesis confirmed by a demonstration that the variation in tetramer coverage of 2-aminobutanoic acid on Pd(111) scales with the increase in enantioselectivity. This is the first clear demonstration of the formation of a chiral template.

To obtain direct evidence that the amino acid tetramer templates form a chiral pocket, we first imaged PO alone on Pd(111) using STM and found that it adsorbs as islands consisting of one-dimensional rows. We then attempted to image PO on amino acid-modified surfaces, but without success. While this effort is ongoing, Figure 4 shows the currently most stable structure, which has dimensions and a simulated STM image (Figure 5) close to that found experimentally.

The enantioselective chemisorption of PO and enantioselective reactivity of 2-butanol were explored on proline modified Pd(111). Proline acted as a chiral modifier for both PO and 2-butanol adsorption and the decomposition of 2-butanol to yield the methylethyl ketone was also found to be enantioselective.

Effect of substrate on enantioselective chemisorption

In order to explore how the nature of the substrate (Pd *vs.* Pt *vs.* Cu, for example) influences the enantioselective interaction between a given chiral template and chiral probe, Tysoe, Zaera and Gellman have studied the enantioselective uptake of R- or S-PO on R- or S-2-butanol templated Pd(111), Pt(111), Cu(111) and Cu(100) substrates. The three surfaces behave differently, with copper showing no enantioselectivity. Zaera and Tysoe have also demonstrated differences in the enantioselective adsorption of PO on Pt(111) and Pd(111) modified with 2-methyl butanoic acid or with NEA.[11-13] An extensive study of Cu(111), Cu(110) and Cu(100) modified with alanine, alaninol, 2-butanol and 2-butoxide and probed with PO and R-3MCHO revealed no enantioselectivity. It was suggested that this arises from the inability of these chiral modifiers to interact with the chiral probes through hydrogen bonding. Substrate effects were further explored by Tysoe on a dilute

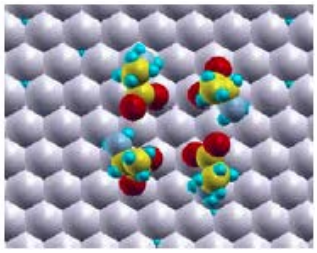
Figure 5. Depiction of the alanine tetramer that has the dimensions and simulated STM image that most closely correspond to the measured images.

Au/Pd(111) alloy containing ~8% gold.[14] Co-adsorption of R-2-butanoxide with R-PO or S-PO leads to enantioselective (*ee* of ~14%) 2-butanone formation that is greater in the presence of *S*-PO than in the presence of *R*-PO. The *ee* values for the formation of 2-butanol from the remaining 2-butoxide species depend strongly on the initial 2-butanoxide coverage, varying from a few percent at moderate coverage, to *ee* ≈ 100 % at low initial 2-butanol coverages.[14]

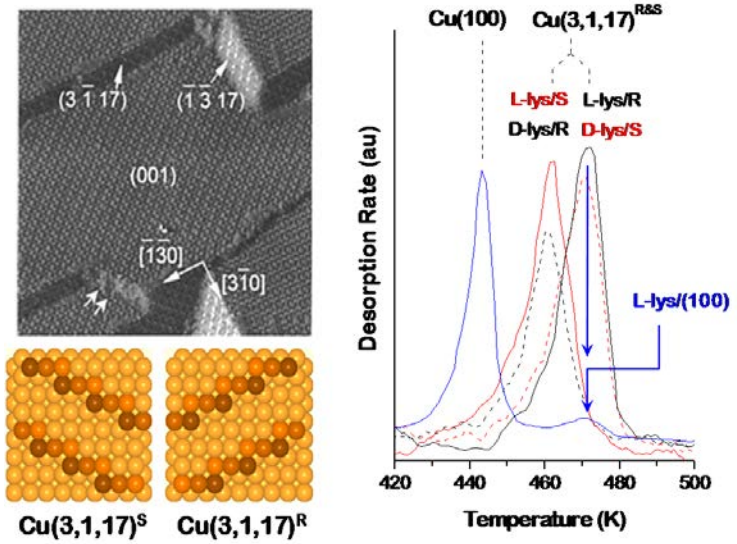

Figure 6. Left panel shows an STM image of the Cu(100) surface modified by the adsorption of L-lysine to create Cu{3,1,17}^{R} facets. The right panel shows the desorption of D- and L-lysine from Cu(100) and Cu(3,1,17)$^{R\&S}$ surfaces. The peak at 472 K for the desorption of L-lysine from the Cu(100) surface is at exactly the same temperature as that for L-lysine desorption from the Cu(3,1,17)^{R} surface.

Propylene oxide on L-lysine/Cu(100): Templating or imprinting?

One of the most intriguing enantiospecific interactions of amino acids on achiral surfaces is the example of L-lysine on Cu(100). Several studies of amino acids on Cu(100) surfaces have used STM to show that amino acids cause a gross reconstruction, leading to the formation of {3,1,17} facets.[15-17] Zhao *et al.* have shown that when L-lysine is adsorbed on the Cu(100) surface it leads to the formation of a homochiral set of {3,1,17}^{R} facets (Figure 6).[16,17] This result indicates that *L*-lysine can be used to *imprint* natural chirality onto an achiral copper surface. This was further explored by showing that that adsorption of PO on Cu(100) modified with *L*-lysine is enantiospecific. The results suggest that the *L*-lysine adsorbs on Cu(100) as a zwitterion, and that this enable hydrogen-bonding interactions to occur with the adsorbed PO. The imprinting of natural chirality into the Cu(100) may also contribute to the enantioselectivity which, in principle, could arise from a combination of both natural chirality and templating effects.

B.4. Accomplishments - One-to-one Chiral Modifiers

Adsorption of cinchonidine on Pt from solution

In order to understand the one-to-one modifier-reactant interaction mechanisms of cinchona alkaloids under realistic conditions, Zaera has used infrared spectroscopy to characterize the adsorption of cinchonidine and related modifiers from solution on platinum surfaces. Its vibrational modes were first assigned using a combination of experimental spectroscopic measurements and *ab initio* computational methods. The geometry of cinchonidine on platinum depends on its concentration in solution; at low and intermediate concentrations, the cinchonidine (Figure 7) is adsorbed with the quinoline ring parallel to the surface but, at high concentrations, the ring tilts away from the surface. The maximum enantioselectivity occurs under conditions consistent with cinchonidine having the quinoline ring parallel to the surface.

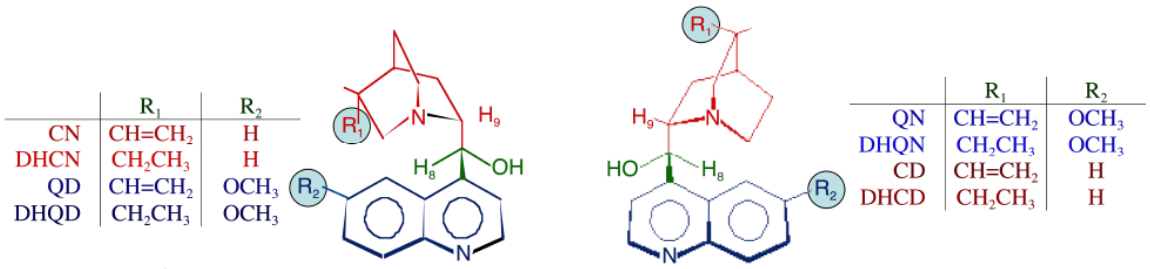

	R_1	R_2
CN	$CH=CH_2$	H
DHCN	CH_2CH_3	H
QD	$CH=CH_2$	OCH_3
DHQD	CH_2CH_3	OCH_3

	R_1	R_2
QN	$CH=CH_2$	OCH_3
DHQN	CH_2CH_3	OCH_3
CD	$CH=CH_2$	H
DHCD	CH_2CH_3	H

Figure 7. Structure of the cinchona alkaloids: cinchonidine, CD; cinchonine, CN; quinine, QN; quinidine, QD; dihydrocinchonidine, DHCD; dihydrocinchonine, DHCN; dihydroquinine, DHQN; and dihydroquinidine, DHQD. These form pairs of 'near' enantiomers that differ only in nature of the peripheral functional groups on the quinuclidine ring (R_1 = H or OCH_3) and quinoline ring (R_2 = $CH=CH_2$ or CH_2CH_3).

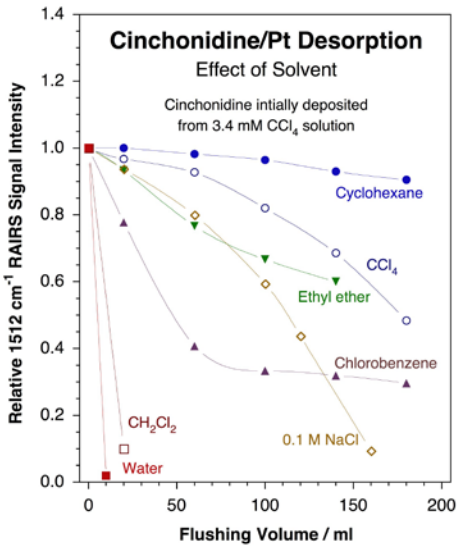

Figure 8. Desorption of adsorbed cinchonidine from a platinum surface into different solvents as a function of rinsing volume. In these experiments the cinchonidine was first adsorbed from a CCl_4-saturated solution, and then flushed with sequential 20 ml aliquots of the stated solvents. The coverage of the adsorbate remaining on the surface was determined *in-situ* by following the infrared absorption signal at 1512 cm^{-1}, which corresponds to an in-plane deformation of the quinoline ring. The data show that the desorption kinetics are very sensitive to the nature of the solvent, varying from fast desorption in water and dichloromethane to irreversible adsorption in cyclohexane and other alkanes. This trend correlates well with the chirality-imparting ability of cinchonidine for enantioselective hydrogenation reactions on platinum catalysts.

The influence of dissolved gases on the orientation of cinchonidine adsorbed onto Pt from CCl_4 solutions was also characterized using FT-IRAS. Most of the gases studied (Ar, N_2, O_2, air and CO_2) have no detectable influence on cinchonidine adsorption. However, hydrogen was found to play a unique role, initially accelerating the uptake of cinchonidine, but later displacing some of the adsorbed cinchonidine from the Pt surface. These results correlate with the effect of the solvent on the enantioselectivity of the Orito reaction. In particular, the effect of solvent polarity on the kinetics of cinchonidine desorption correlated with the solvent influence on the enantioselectivity of the Orito reaction on the cinchonidine-modified Pt catalyst. Cinchonidine adsorbs irreversibly on Pt from non-polar solvents such as cyclohexane, but can be removed easily by more polar solvents such as CH_2Cl_2. The evolution of the adsorbed cinchonidine overlayer on Pt during flushing with different solvents is illustrated in Figure 8. The cinchonidine solubility correlates well with the activity and enantioselectivity of the cinchonidine/Pt catalyst for the Orito reaction. In general, the enantioselective properties of the cinchonidine/Pt catalyst are defined by the adsorption geometry of the cinchonidine modifier which, in turn, is influenced by reaction parameters such as the cinchonidine concentration, the type of solvent, and the nature of the gases dissolved in the liquid phase.

The next stage of the investigation was to understand the effects of the cinchona modifier's molecular structure on its adsorption and ability to

impart catalytic enantioselectivity to the Orito reaction. A comparative study using cinchonidine, cinchonine, quinine, quinidine, and the dihydro analogs of those four molecules revealed that the adsorption equilibrium constants (K_{ads}) followed the sequence cinchonine > quinidine > cinchonidine > quinine (Figure 9). Some of this ordering can be explained by solubility differences, but quinidine has a much larger K_{ads} than expected from its relatively high solubility; bonding to the surface must also play a role in determining the trends in K_{ads}. FT-IRAS experiments revealed that each of the cinchona alkaloids binds differently on platinum at saturation coverage; while the quinoline ring of cinchonidine tilts along its long axis to optimize π-π intermolecular interactions, in cinchonine it tilts along the short axis and bonds to the surface through the lone electron pair of the nitrogen atom. Both quinine and quinidine exhibit additional bonding interactions with the surface *via* their methoxy oxygen atoms. Perhaps a more surprising result from this work is the fact that cinchonine displays a higher K_{ads} than cinchonidine, quinine or quinidine in spite of the fact that, according to previous work, it can be readily displaced from the surface by all of those cinchona alkaloids.

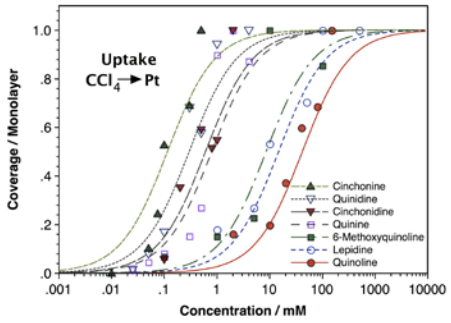

Figure 9. Adsorption isotherms for several cinchona and related compounds from solution onto a platinum surface, as determined by *in-situ* infrared spectroscopy detection.

The variations between the different cinchona alkaloids, both in their adsorption properties, and in their behavior in solution were deemed to arise from intrinsic molecular properties associated with their structure: the relative solubilities of the different cinchona alkaloids are roughly independent of solvent type (Figure 8). Correlations between the cinchona conformations and their chemical behavior have already been identified in some cases, but not yet fully explained. Preliminary NMR and DFT data suggest that the most stable configuration may be determined by the steric effects exerted by the peripheral functional groups (vinyl, methoxy) bonded to the quinuclidine and quinoline rings. This behavior may account for the reported differences in catalytic enantioselectivities observed when using cinchonidine and cinchonine as chiral modifiers.

In studies of cinchona alkaloids as one-to-one chiral modifiers, we have shown that subtle changes in the position of the substituent groups outside the central chiral pocket explain the basic physicochemical differences between pairs of near-enantiomers (quinine *vs.* quinidine, cinchonidine *vs.* cinchonine). Such properties include crystal structure, solubility, and adsorption equilibrium. Both energetic and entropic factors must be considered to fully account for the observed trends. These studies involved eight cinchona compounds, and a comparative study based on a combination of quantum mechanical calculations, solubility measurements, NMR configurational analyses, and *in-situ* characterization of the adsorption of those compounds on solid surfaces using infrared absorption spectroscopy. Two factors are considered: the rotational configuration of each molecule in the gas *versus* the solid state, and the intermolecular interactions that hold the crystal together. Particularly puzzling is the fact that, although cinchonidine and cinchonine are near enantiomers, they crystallize in different structures. Our data indicate that this is mostly due to intermolecular interactions, arising from the better packing available to cinchonine, possibly because of the position of the peripheral vinyl group relative to that in cinchonidine. It is this subtle effect of the outside moieties of these molecules that we believe defines many of their unique enantiospecific properties.

UHV adsorption of NEA and MP on Pd(111) and Pt(111)

Our studies on the adsorption of cinchona alkaloids and their analogs from solution are complemented by surface-science studies of a close analog, NEA, on Pt(111) and Pt(111) surfaces. Solution-phase experiments on cinchona alkaloids discussed above provide detailed information on the effects of solvents on the structure and adsorption properties of cinchona alkaloids, but these systems are sufficiently complex that the interactions between the cinchona modifier and prochiral reactant and product (alkyl pyruvate and lactate, respectively) in the Orito reaction cannot be explored in detail. The UHV experiments study enantiospecific adsorbate-adsorbate interactions using NEA co-adsorbed with chiral probes, such as PO, or the prochiral reactants and products of the Orito reaction.

The surface chemistry of methyl pyruvate (MP) and methyl lactate (ML) was studied on Pd(111) by Tysoe. MP adsorbs at low coverages with its molecular plane parallel to the surface, and reorients to be perpendicular to the surface as the coverage increases, and some spectroscopic evidence is found for the presence of the enol form of MP. A portion of the flat-lying MP decomposes at higher temperatures to form an adsorbed pyruvate species. The structure of MP has been calculated on Pd(111) by DFT methods, which predict heats of adsorption of flat-lying and perpendicular MP that are in good agreement with the desorption activation energies measured by TPD.[37] The chemistry of ML on Pd(111) is similar to that of MP; ML either desorbs, or dehydrogenates to form flat-lying MP, which subsequently decomposes in an identical manner to that found for flat-lying MP on Pd(111). We have collected STM images of MP on Pd(111) (Figure 10), which display all forms of MP that have been identified spectroscopically. The enol form was assigned by comparison with previous images on Pt(111), and the flat-lying species was simulated using bSKAN. The assignment of the vertical form of MP was confirmed by imaging it on a CO-covered surface to force it into an upright configuration.

We have also explored the chemistry of NEA on

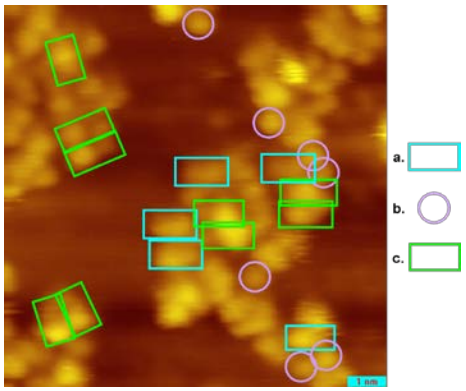

Figure 10. A high-resolution STM image of methyl pyruvate on Pd(111) at 120 K showing the various forms on methyl pyruvate on the surface. Examples of flat-lying methyl pyruvate are enclosed by blue boxes (a), the vertical forms by purple circles (b) and the enol by green rectangles (c).

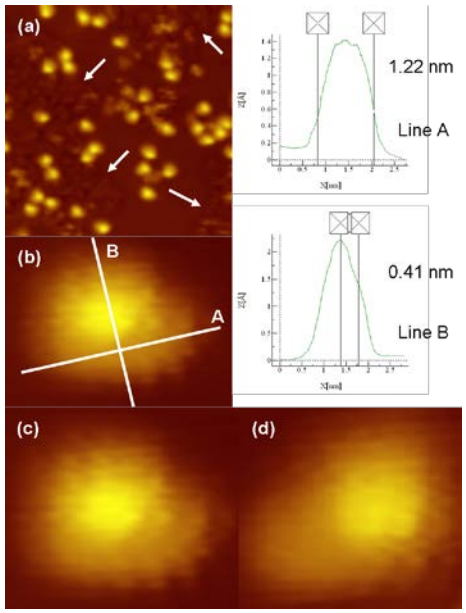

Figure 11. (a) 20.1 nm×20.1 nm STM image of NEA on Pd(111) at low coverage (relative coverage θ = 0.057 ML) taken at 100 K. The line profiles along the white lines (b) are shown on the right and correspond to a molecule along its long axis (top) and perpendicular to it (bottom). (c) and (d) display the two conformers of NEA. Imaging conditions: V_b = -101 mV; current set point I_t = 19.3 pA.

Pd(111) surfaces using TPD and RAIRS, coupled with DFT calculations, to show that it bonds through the naphthyl ring, which lies parallel to the surface, similar to the structure of the most enantioselective orientation of cinchonidine. These results are corroborated by STM images of NEA on Pd(111) (an example of which is shown in Figure 11). This further reveals that the NEA is randomly distributed on the surface, as was found on Pt(111), consistent with a one-to-one interaction. Both *exo* and *endo* conformers of NEA were identified by STM and the measured coverage ratio of the two conformations was rationalized using Monte Carlo methods. Similar surface chemistry has been found for NEA on Pt(111).

Enantioselective adsorption of chiral probes with one-to-one modifiers.

We have found enantioselective adsorption of chiral probes with NEA on both Pt(111) and Pd(111) surfaces. On NEA-modified Pd(111), Tysoe found enantioselective adsorption of 2-butanol over a narrow NEA coverage range suggestive of templating effects. These results, however, appear to be inconsistent with the observed random distribution of NEA on Pd(111). Evidence was obtained on Pt(111) by Zaera for both 1:1 complexation and templating contributions to enantioselective adsorption. We have explored the adsorption of NEA on Pt(111) by RAIRS and TPD under ultrahigh vacuum and also *in situ* from liquid solutions. Evidence was obtained for both the formation of supramolecular chiral templates and the complexation of individual modifiers with the MP reactant. In particular, TPD titrations of NEA-modified Pt(111) using PO as a chiral probe pointed to a relative enhancement in the adsorption of one enantiomer over the other at intermediate NEA coverages, the behavior expected from the templating mechanism. On the other hand, an enantiospecific difference in R- and S-PO adsorption energetics was also observed. Both TPD and RAIRS data suggested enantiospecific interactions between the adsorbed NEA and adjacent PO. The NEA uptake from solution displayed additional enantioselectivity, in particular when comparing the adsorption of enantiomerically pure NEA with that of racemic mixtures, and also pointed to possible adsorption changes induced by ethyl pyruvate, a common reactant in chiral hydrogenation processes.

In order to understand the NEA-induced enantioselectivity of PO adsorption, we have (in collaboration with Zgrablich) developed molecular models based on Monte Carlo simulations for PO on Pt(111) modified by NEA. The observed enantioselectivity could not be explained simply by pair-wise interactions between co-adsorbed PO and NEA, but rather required the inclusion of co-operative effects. Starting from a very simple model, kinetic Monte Carlo simulations were able to predict the TPD spectra of PO from surfaces modified with different coverages of NEA that required the inclusion of quite complex interactions to satisfactorily reproduce the experimental data. Finally, Tysoe has studied the enantioselective adsorption of ML on NEA-covered surfaces. The enantioselectivity increased over a narrow NEA coverage range, showing a sharp peak at a NEA coverage of ~0.6 ML.

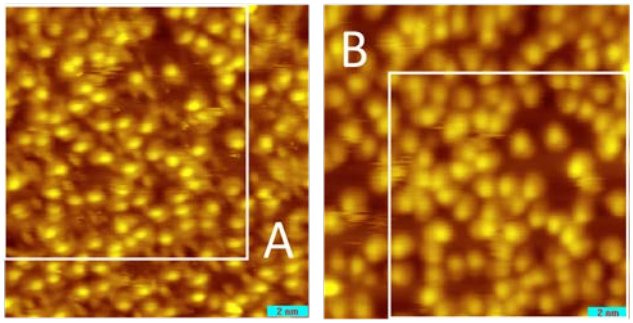

Figure 12. High-resolution STM image of MP with NEA on Pd(111) at 120 K. Two types of image were detected. Image A shows the surface before tip cleaning and image B afterwards. The white boxes define identical scan areas.

Identification of prochiral docking complexes

Tysoe has collected STM images of MP adsorbed on NEA-covered Pd(111) at 120 K (Figure 12). The image in Figure 12A shows a diffuse region that contains a bright protrusion and a dark spot. The image in Figure 12B is a subsequent scan collected after cleaning the STM tip, which shows an extended region with a brighter spot at one end. The white squares outline exactly identical scanning areas where there is a direct correspondence between the structures in both images. Thus, the image in Figure 12A is collected with a functionalized tip (likely by MP) while the image in Figure 12B is obtained with a clean one. Such differences between the images of identical species have been observed previously on reactive metal surfaces, for example, for acetophenone on Pt(111). In that case, the dark spot corresponded to the presence of the carbonyl group, which may aid in assigning the docking complex in our work. An example of a higher-resolution image is shown in Figure 13, along with two profiles along the lines indicated by A and B, where the images were collected with a clean tip. The profile along A yields a width of ~1.3 nm, corresponding to the distance along the long axis of the naphthyl group (which is oriented along the close-packed $<1\bar{1}0>$ rows) and is identical to that found for NEA alone (Figure 11) allowing the location of the naphthyl group to be identified. However, the distance along profile B is ~1.9 nm, substantially larger than for NEA alone, due to the presence of MP.

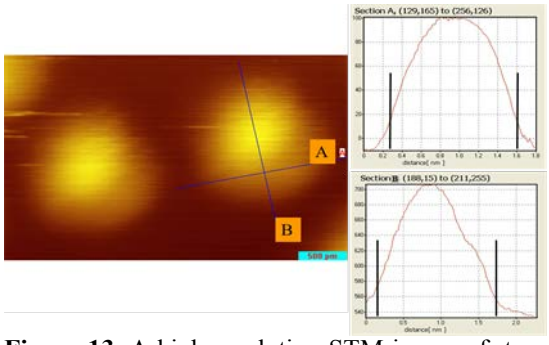

Figure 13. A high-resolution STM image of two structures formed by co-adsorbing methyl pyruvate and NEA on Pd(111) at 120 K along with the profiles measured along the lines A and B.

Recent STM work by McBreen identified docking complexes between trifluoroacetophenone (TFAP) and NEA on Pt(111) where the images are a simple sum of the individual components. However, the images shown in Figures 12 and 13 are not a simple superposition of those of NEA and MP alone. Tysoe recently carried out TPD experiments for MP co-adsorbed with NEA on deuterium-covered Pd(111). The surface was pre-dosed with deuterium to minimize MP decomposition. Predominantly perpendicular MP was identified from its characteristic desorption temperature. More interestingly, H-D exchange (but not complete hydrogenation) of the MP was also found in the CH_3-C=O group where the extent of H-D exchange varied with NEA coverage, reaching a maximum at ~0.5 ML. Such H-D exchange has been seen previously for MP on Pt(111) and proposed to occur *via* the enol form. These results imply that the docking complex involves a vertically oriented MP and that its rate of H-D exchange is enhanced by the presence of NEA.

B.5. Accomplishments - Chiral Materials Synthesis

Tethering cinchona alkaloids

As mentioned earlier, the Orito reaction uses a chiral cinchona modifier in solution with a particulate platinum catalyst for enantioselective hydrogenation of α-ketoesters to chiral alcohols. In Zaera's lab, cinchona alkaloid modifiers have been tethered to high-surface-area silica supports, with the ultimate goal of combining them with platinum nanoparticles to obtain the enantioselective behavior of cinchona normally added as a chiral modifier in solution. If successful, this approach will lead to a heterogeneous chiral catalyst that does not require the

addition of chiral modifiers to the reacting solution. Two routes for tethering cinchona have proven to be viable. The most effective was one in which cinchonidine is first derivatized with 3-isocyanatopropyltriethoxysilane (ICPTEOS) at the alcohol position, and then anchored to the silica surface *via* the triethoxysilane group. Tethering occurs *via* the formation of Si-O-Si bonds at silica sites having two geminal hydroxyl groups on the same silicon atom. The resulting catalyst was successfully tested for the enantioselective addition of aromatic thiols to unsaturated ketones. The activity of the supported cinchonidine catalyst proved to be comparable to that of a platinum catalyst with the free modifier in solution, but tethering does lead to a significant loss of enantioselectivity.

Chirally modified gold nanoparticles

The rapid recent advances in the synthesis and characterization of shape-controlled metal nanoparticles have put the synthesis of chiral nanoparticles with controlled enantioselectivity within reach. Gellman and collaborated with Shukla to prepare chiral Au nanoparticles and demonstrated their enantioselective adsorption of several chiral probes: PO, 2-butanol, and glucose. The Au nanoparticles are rendered chiral by templating their surfaces with chiral ligands such as D- or L-cysteine. We have developed a very simple polarimetry experiment for detecting their enantiospecific adsorption of chiral probes. As illustrated in Figure 14A, adding a racemic mixture of a chiral probe such as PO to a solution containing enantiomerically pure, chiral Au nanoparticles results in a partitioning of the PO between the solution and an adsorbed phase. If the equilibrium constants for adsorption are enantiospecific, $K_D^R \neq K_D^S$ or $K_L^R \neq K_L^S$, then the concentrations of the two probe enantiomers in solution and in the adsorbed phase will differ. A key element of this experiment is that once adsorbed on Au nanoparticles, the optical rotation constant of PO differs from that in solution; in this case, it is higher. This phenomenon, first demonstrated by Shukla, is critical because it provides contrast between the optical rotation of light by the adsorbed- and solution-phase PO. As result, when racemic-PO is added to a solution

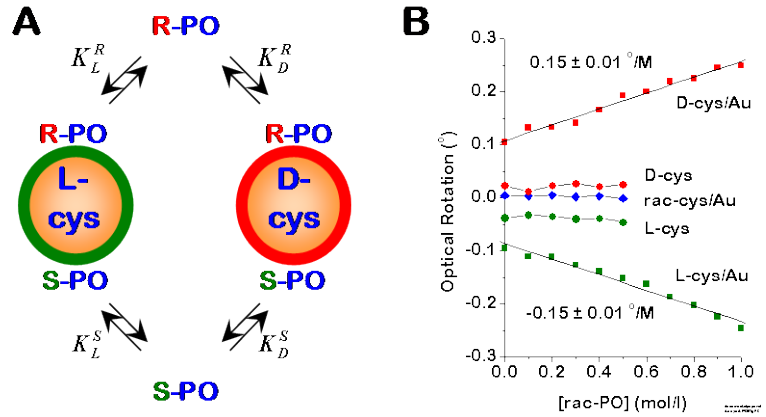

C

Parameter		Value
α_{sol}^S	$-\alpha_{sol}^R$	0.90 ± 0.04 °/M
α_{ads}^S	$-\alpha_{ads}^R$	2.2 ± 0.3 °/M
K_D^R	K_L^S	8 ± 3 /M
K_L^R	K_D^S	50 ± 1 /M
S_0		0.23 ± 0.07 M

Figure 14. A) Gold nanoparticles modified with D- or L-cysteine and in the presence of R- or S-PO. The equilibrium constants, $K_{D/L}^{R/S}$, describe the adsorption of the R- or S- PO on the surfaces of the D- or L-cys modified nanoparticles. B) Optical polarimetry of gold nanoparticles during addition of rac-PO to solution. The equal and opposite slopes when added to D- or L-cys/Au indicate enantioselective partitioning of the enantiomers between solution phase and adsorbed onto the particles. Parameter estimates for the optical rotation constants, $\alpha_{sol/ads}^{R/S}$; adsorption equilibrium constants, $K_{D/L}^{R/S}$; and concentrations of adsorption sites, S_0, on the gold nanoparticles, all derived from polarimetry data.

of chiral Au nanoparticles, enantiospecific adsorption results in a net rotation of polarized light (Figure 14B). Note that, when the Au nanoparticles are modified by a racemic mixture of DL-cysteine, or when there is only D- or L-cysteine in solution without Au nanoparticles, the addition of racemic PO to solution does not result in any optical rotation.

Gellman has developed a simple, quantitative model for enantiospecific adsorption on chiral gold nanoparticles and for predicting the consequent optical rotation. This model has been used to analyze the data shown in Figure 14B. A number of calibration measurements were used to derive the estimates shown in Figure 14C for the enantiospecific adsorption equilibrium constants, $K_{D/L}^{R/S}$, the optical rotation constants for PO, $\alpha_{sol/ads}^{R/S}$, and the concentration of adsorption sites on the gold nanoparticles, S_0. The beauty of these experiments is that these quantities can be determined solely on the basis of a set of careful measurements of optical rotation. In fact, all of the syntheses and optical rotation measurements were made by an undergraduate student working with Shukla and they are well within the capability of good undergraduate researchers.

Chiral imprinting of metals

In addition to templating, chiral adsorbates on metal surfaces can induce surface chirality by imprinting; the reconstruction of the surface to form naturally chiral facets. In early work on Cu(221) surfaces, Gellman and collaborators observed the reconstruction of achiral steps to form kinked step edges during adsorption of R-3MCHO at 300 K. At the same time, Zhao *et al.* reported the STM image in Figure 6 revealing the reconstruction of Cu(100) to expose Cu{3,1,17}facets following L-lysine adsorption. Although both $Cu\{3,1,17\}^S$ and $Cu\{3,1,17\}^R$ facets are possible, they observed only $Cu\{3,1,17\}^R$ facets. This is a very exciting observation of chiral imprinting.

Recently, Gellman completed a detailed study of D- and L-lysine adsorption and desorption from Cu(100) and $Cu(3,1,17)^{R\&S}$ surfaces. L-lysine desorbs molecularly from these surfaces and its desorption energetics are consistent with Zhao's observation of chiral imprinting, in the sense that the desorption energies estimated from the TPD spectra (Figure 6) follow the trend $\Delta E_{(100)}^{L-\text{lys}} < \Delta E_{(3,1,17)\text{S}}^{L-\text{lys}} < \Delta E_{(3,1,17)\text{R}}^{L-\text{lys}}$. In other words, these energy differences provide the driving force for reconstructing the Cu(100) surface, and for the preference of L-lysine to produce R- rather than S-facets. Equally important, the desorption temperatures for D- and L-lysine from $Cu(3,1,17)^{R\&S}$ demonstrate that the desorption energies exhibit diastereomerism, $\Delta E_{(3,1,17)\text{R}}^{D-\text{lys}} = \Delta E_{(3,1,17)\text{S}}^{L-\text{lys}} \neq \Delta E_{(3,1,17)\text{R}}^{L-\text{lys}} = \Delta E_{(3,1,17)\text{S}}^{D-\text{lys}}$, as they must. Furthermore, the desorption spectra of D- and L-lysine from the Cu(100) surface both show weak, high-temperature desorption features at 472 K, the temperatures at which D- and L-lysine desorb from the $Cu(3,1,17)^S$ and $Cu(3,1,17)^R$ surfaces, respectively (Figure 6). These features are believed to arise from the imprinted facets observed by Zhao. The combined evidence for chiral imprinting is extremely exciting because it suggests a pathway to synthesize naturally chiral metal surfaces from achiral metals.

References

(1) McFadden, C. F.; Cremer, P. S.; Gellman, A. J. *Langmuir* **1996**, *12*, 2483.

(2) Horvath, J. D.; Baker, L.; Gellman, A. J. *J. Phys. Chem. C* **2008**, *112*, 7637.

(3) Huang, Y.; Gellman, A. J. *Catal. Lett.* **2008**, *125*, 177.

(4) Sholl, D. S.; Asthagiri, A.; Power, T. D. *J. Phys. Chem. B* **2001**, *105*, 4771.

(5) Baber, A. E.; Gellman, A. J.; Sholl, D. S.; Sykes, E. C. H. *The Journal of Physical Chemistry C* **2008**, *112*, 11086.

(6) Baker, L.; Holsclaw, B.; Baber, A. E.; Tierney, H. L.; Sykes, E. C. H.; Gellman, A. J. *J. Phys. Chem. C* **2010**, *114*, 18566.

(7) Xu, F.; Huang, Y.; Pushkarev, V.; Gellman, A. J. **2009**, to be published.

(8) Gao, F.; Wang, Y. L.; Burkholder, L.; Tysoe, W. T. *Surface Science* **2007**, *601*, 3579.

(9) Gao, F.; Li, Z. J.; Wang, Y. L.; Burkholder, L.; Tysoe, W. T. *Surface Science* **2007**, *601*, 3276.

(10) Gao, F.; Li, Z. J.; Wang, Y. L.; Burkholder, L.; Tysoe, W. T. *J. Phys. Chem. C* **2007**, *111*, 9981.

(11) Burkholder, L.; Stacchiola, D.; Boscoboinik, J. A.; Tysoe, W. T. *Journal of the American Chemical Society* **2009**, submitted.

(12) Lee, I.; Ma, Z.; Kaneko, S.; Zaera, F. *Journal of the American Chemical Society* **2008**, *130*, 14597.

(13) Lee, I.; Zaera, F. *Journal of the American Chemical Society* **2006**, *128*, 8890.

(14) Gao, F.; Wang, Y. L.; Li, Z. J.; Furlong, O.; Tysoe, W. T. *J. Phys. Chem. C* **2008**, *112*, 3362.

(15) Chen, Q.; Richardson, N. V. *Progress in Surface Science* **2003**, *73*, 59.

(16) Zhao, X. Y. *Journal of the American Chemical Society* **2000**, *122*, 12584.

(17) Zhao, X. Y.; Zhao, R. G.; Yang, W. S. *Langmuir* **2000**, *16*, 9812.

C. Current and pending support

DOE: "Molecular Level Design of Heterogeneous Chiral Catalysts"; $1,980,000; 09/14/09-08/13/12; (PI: Gellman, co-PIs: D.S. Sholl, W.T. Tysoe, F. Zaera)

Gellman

1. NSF, "MRI: Development of instrumentation for high throughput surface science and materials science studies of multicomponent alloys" $634,599, 2009 – 2011, NSF CBET-0923083 (PI with co-PIs G. Rohrer, R. Davis, J.B. Miller, J. Kitchin)
2. NSF, "Collaborative research: High throughput structure sensitive surface chemistry" $790,000, 2010 – 2013, NSF CHE-1012358, (PI with co-PIs E.C. Sykes, D.S. Sholl)
3. NSF, "Development of Pd Alloy Membranes for Ultrapure Hydrogen Production" $300,000, 2010 – 2013, NSF CBET-1033804 (co-PI with J.B. Miller)
4. DOE NETL-RUA "Surface structure sensitivity of FT and RWGS catalysis - High throughput studies" $300,000, 2011
5. DOE NETL-RUA "High-Permeance, Poison Tolerant Alloys for Hydrogen Separation Applications" $300,000, 2011(co-PI with J.B. Miller)

Sholl

1. National Science Foundation, "NIRT: Gated Transport Through Carbon Nanotube Membranes" $200,000, 8/7 – 7/11 (C. Grigoropoulos (Berkeley) is PI, Bakajin (LLNL) and Sholl are co-PIs)
2. NSF, "Collaborative research: High throughput structure sensitive surface chemistry" $790,000, 2010 – 2013, NSF CHE-1012358, (PI with co-PIs E.C. Sykes, D.S. Sholl)
3. DoE, "Ab initio screening of alloys for hydrogen purification membranes", $450,000, 8/08 – 7/11
4. Dow Corporation, "Ethanol, Propanol and other high alcohol synthesis from H_2/CO, a combined experimental and Computational Approach", $1,184,000, 9/8 – 8/11 (C. Jones is PI, Sholl is 1 of 2 Co-PIs)
5. Conoco Phillips Corp, "Advanced Materials and Membranes for Gas Separations" $2,376,656, 10/08 – 10/12 (S. Nair is PI, Sholl is one of 4 co-PIs)
6. DoE-BES (EFRC Program), "Catalysis by design – combining experiments and theory for energy applications", $711,402 (GT Share), 7/09 – 6/14 (J. Spivey (LSU) is PI, Sholl is one of 18 co-PIs and other senior personnel)
7. SWRI (DoE-NETL), "Amorphous Alloy Membranes for High Temperature Hydrogen Separations", $507,587, 1/10 – 12/12
8. DoE-NETL, "High-performance Sorbents for Carbon Dioxide capture from Air", $299,831, 1/10 – 12/12
9. National Science Foundation, "Unlocking the Potential of MOFs as Membranes using Coupled Modeling and Experiments", $300,000, 6/10 – 6/12

Tysoe

1. Molecular-level Design of Heterogeneous Chiral Catalysts, 9/15/2009-9/14/2012, $395,001, W.T. Tysoe, Co-P.I. with Z. Zaera at UC-Riverside, A. Gellman at Carnegie-Mellon University and D. Scholl at Georgia Institute of Technology.
2. Understanding the Frictional Properties of Boundary Films, 7/11/2008-7/12/2011, $532,867, National Science Foundation, W.T. Tysoe, P.I.
3. Study of the Tribological Properties of Parylene Films, December 2008-June 2011, $25,000, Whirlpool Corporation, W.T. Tysoe, P.I.
4. Environmentally Friendly h-BN Engine Lubricant Additives and Wear Inhibitors, September 2011-August 2014, $1,002,718, Department of Energy, W.T. Tysoe, P.I. in collaboration with Benz Oil, Inc, Argonne National Laboratory.
5. NEB: Nanodevices by Self Assembly of Isocyanide Functionalized Polyaromatic Molecules, August 2011-July 2015, $1,995,010, National Science Foundation, W.T. Tysoe, P.I. in collaboration with Brookhaven National Laboratory and Northwestern University.
6. An Ultrahigh Vacuum Investigation of Shear-Induced Tribological Surface Chemistry, May 2011 - April 2014, $481,757, National Science Foundation, W.T. Tysoe, P.I.
7. Surface Reaction Pathways on Model Gold Palladium Alloy Catalysts, May 2011 - April 2014, $546,642, National Science Foundation, W.T. Tysoe, P.I.
8. Design of Novel Catalyst Structures by Embossing, January 2012 - December 2013, $100,000, ACS Petroleum Research Fund, W.T. Tysoe, P.I.

Zaera

1. NSF - CBET: "Size and Shape Control in Heterogeneous Catalyst Synthesis"; $330,000; 07/01/08 - 06/30/11
2. DOE: "Atomic Layer Deposition (ALD) of Metal and Metal Oxide Films: A surface science Study"; $558,000; 08/15/09 – 08/14/12
3. Intel/UC-Discovery: "Surface Science Studies of CVD and ALD Processes for Ru Deposition"; $675,208; 10/01/09 – 09/30/12
4. DOE: "SISGR: Design and Characterization of Novel Photocatalysts with Core-Shell Nanostructures" (F. Zaera, PI, C. J. Bardeen and Y. Yin, Co-PIs); $1,120,000; 09/15/09 – 09/14/12
5. NSF - MRI: "MRI-R2: Acquisition of an X-Ray Photoelectron Spectrometer (XPS)" (Zaera, PI, D. B. Bocian, R. C. Haddon, M. Ozkan, Y. Yan, Co-PIs); $1,000,000; 04/15/10 – 03/31/13
6. Air Products: "Characterization of the surface chemistry of novel strontium compounds in connection with their use as precursors for the chemical deposition of thin films"; $70,000; 04/01/11 - 09/30/11

D. Publication List

Papers Solely Funded by This Grant

1. Formation of Chiral Templates from Amino Acids on a Pd(111) Surface, Luke Burkholder, Mausumi Mahapatra, Anibal Boscoboinik, Yun Bai and Wilfred T. Tysoe, in preparation

2. W.Y. Cheong, A.J. Gellman "Enantiospecific desorption of R- and S-propylene oxide from D- or L-lysine Modified Cu(100) Surfaces" *Langmuir*, **28,** (2012), 15251−15262

3. Y. Yun, A.J. Gellman, "Enantioselective separation of DL-aspartic acid on naturally chiral Cu(3,1,17)$^{R\&S}$ surfaces" *Angewandte Chemie International Edition*, in preparation

4. B. Mahtre, V.V. Pushkarev, B. Holsclaw, T.J. Lawton, E.C.H. Sykes, A.J. Gellman, "A Window on Surface Explosions: Tartaric Acid on Cu(110)" *Journal of Physical Chemistry C*, in press

5. A.J. Gellman, Y. Huang, F. Xu, V.V. Pushkarev, B. Holsclaw, B. Mhatre, "Super-enantioselective chiral surface explosions" in preparation

6. Junghyun Hong, Ilkeun Lee, and Francisco Zaera, Cinchona Alkaloids Anchored on Porous Silica as Enantioselective Heterogeneous Catalysts, *Top. Catal.*, **54(19/20)**, 1340-1347 (2011). INVITED (Special Issue, Chiral Surface Chemistry and Catalysis)

7. Junghyun Hong and Francisco Zaera, Interference by the Solid on the Performance of Tethered Molecular Catalysts, *J. Am. Chem. Soc.*, **134(31)**, 13056–13065 (2012)

8. Alexander D. Gordon and Francisco Zaera, Adsorption of 1-(1-Naphthyl)ethylamine from Solution onto Pt Surfaces: Implications for the Chiral Modification of Heterogeneous Catalysts, *Angew. Chem., Int. Ed.*, submitted

9. N. Ondeck, N. Khosla, S. Klara, P. Downey, A. Petti, N. Shukla, A.J. Gellman "Effect of wavelength and temperature on measurements of optical rotation during enantiospecific adsorption on chiral Au nanoparticles" in preparation

10. N. Ondeck, N. Khosla, N. Shukla, A.J. Gellman "Quantitative analysis of optical rotation measurements of chiral probe molecules adsorbed on chiral metal nanoparticles" in preparation

Papers Jointly Funding by DOE (including other DOE grants) and other Federal or Non-Federal Sources

1. W.D. Michalak, J.B. Miller, C. Yoclu, A.J. Gellman "Fabrication of metallic nanoparticles by spinodal dewetting of thin films: A high-throughput approach" *Thin solid Films* **522,** (2012), 473-479

2. F. Braun, J.B. Miller, A.J. Gellman, A.M. Tarditi, B. Fleutot, P. Kondrayuk, L.M. Cornaglia, "PdAgAu alloy with high resistance to corrosion by H_2S" *International Journal of Hydrogen Energy*, **37(23**), (2012), 18547-18555

3. P. Kondratyuk, G. Gumuslu, S. Shukla, J.B. Miller, B.D. Morreale, A.J. Gellman "A Microreactor Array for Spatially-Resolved Measurement of Catalytic Activity on Composition Spread Alloy Films: a Device for High-Throughput Catalyst Evaluation" *Journal of Catalysis*, in preparation

4. W.D. Michalak, A.J. Gellman, "Reaction Path Analysis of Dynamic Systems: Identifying the Dominant Transition and Intermediate States" *Journal of Physical Chemistry B,* submitted

5. Francisco Zaera, Surface Chemistry at the Liquid/Solid Interface, *Surf. Sci.*, **605(13/14)**, 1141-1145 (2011). INVITED, PROSPECTIVE

6. Menno Bouman and Francisco Zaera, Reductive Eliminations from Amido Complexes, *J. Electrochem. Soc.*, **158(8)**, D524-D526 (2011).

7. Qiao Zhang, Diana Q. Lima, Ilkeun Lee, Francisco Zaera, Miaofang Chi and Yadong Yin, A Highly Active TiO_2-Based Visible-Light Photocatalyst with Nonmetal Doping and Plasmonic Metal Decoration, *Angew. Chem., Int. Ed.*, **50(31)**, 7088-7092 (2011).

8. Qiang Ma, Roy G. Gordon, and Francisco Zaera, Surface Chemistry of Copper(I) Acetamidinates in Connection with Atomic Layer Deposition (ALD) Processes, *Chem. Mater.*, **23(14)**, 3325-3334 (2011).

9. Huaxing Sun, Xiangdong Qin, and Francisco Zaera, Chemical Nature of the Thin Films that Grow on SiO_2/Si(100) Surfaces Upon Manganese Deposition, *J. Phys. Chem. Lett.*, **2 (20)**, 2525–2530 (2011).

10. Ilkeun Lee, Ji Bong Joo, Yadong Yin and Francisco Zaera, A New Yolk@Shell Nanoarchitecture for Au/TiO_2 Catalysts, *Angew. Chem., Int. Ed.*, **50(43)**, 10208–10211 (2011). INVITED

11. Xiangdong Qin, Huaxing Sun, and Francisco Zaera, Thermal Chemistry of $Mn_2(CO)_{10}$ during Deposition of Thin Manganese Films on Silicon Oxide and on Copper Surfaces, *J. Vac. Sci. Technol. A*, **30(1)**, 01A112/1-01A112/10 (2012). SPECIAL ISSUE: ALD

12. Qiang Ma, Roy G. Gordon, and Francisco Zaera, Thermal Chemistry of Copper(I)-N,N'-di-sec-butylacetamidinate on Cu(110) Single-Crystal Surfaces, *J. Vac. Sci. Technol. A*, **30(1)**, 01A114/1-01A114/10 (2012). SPECIAL ISSUE: ALD

13. Ji Bong Joo, Qiao Zhang, Ilkeun Lee, Michael Dahl, Francisco Zaera, and Yadong Yin, Mesoporous Anatase Titania Hollow Nanostructures though Silica-Protected Calcination, *Adv. Funct. Mater.*, **22**, 166-174 (2012).

14. Ji Bong Joo, Qiao Zhang, Michael Dahl, Ilkeun Lee, James Goebl, Francisco Zaera, and Yadong Yin, Control of the Nanoscale Crystallinity in Mesoporous TiO_2 Shells for Enhanced Photocatalytic Activity, *Energy Environ. Sci.*, **5**, 6321-6327 (2012).

15. Taeseung Kim and Francisco Zaera, X-Ray-Initiated Metal-Promoted Thin Film Growth, *J. Phys. Chem. C*, **116(15)**, 8594-8600 (2012).

16. Francisco Zaera, The Surface Chemistry of Atomic Layer Depositions of Solid Thin Films, *J. Phys. Chem. Lett.*, **3**, 1301-1309 (2012). INVITED

17. Francisco Zaera, New Challenges in Heterogeneous Catalysis for the 21st Century, *Catal. Lett.*, **142(5)**, 501-516 (2012). INVITED PERSPECTIVE

18. Francisco Zaera, Probing Liquid/Solid Interfaces at the Molecular Level, *Chem. Rev.*, **112(5)**, 2920–2986 (2012).

19. Xiaoliang Liang, Jie Li, Ji Bong Joo, Alejandro Gutiérrez, Aashani Tillekaratne, Ilkeun Lee, Yadong Yi, and Francisco Zaera, Diffusion through the Shells of Yolk@Shell and Core@Shell Nanostructures in Liquid Phase, *Angew. Chem., Int. Ed.*, **51(32)**, 8034-8036 (2012).

20. Huaxing Sun, Xiangdong Qin, and Francisco Zaera, Activation of Metalorganic Precursors by Electron Bombardment in the Gas Phase for Enhanced Deposition of Solid Films, *J. Phys. Chem. Lett.*, **3**, 2523–2527 (2012).

21. Francisco Zaera, Infrared Absorption Spectroscopy of Adsorbed CO: New Applications in Nanocatalysis for an Old Approach, *ChemCatChem*, **4(10)**, 1525-1533 (2012). INVITED

22. Qiang Ma and Francisco Zaera, The Chemistry of $Cu(acac)_2$ on Ni(110) and Cu(110) Surfaces: Implications for Atomic Layer Deposition (ALD) Processes, *J. Vac. Sci. Technol. A*, in preparation.

23. Huaxing Sun and Francisco Zaera, Chemical Deposition of Manganese Metallic Films on Silicon Oxide Substrates, *J. Phys. Chem. C.*, **116 (44)**, 23585–23595 (2012).

24. Robert J. Dillon, Ji-Bong Joo, Francisco Zaera, Yadong Yin, and Christopher J. Bardeen, Correlating the excited state relaxation dynamics as measured by photoluminescence and transient absorption with the photocatalytic activity of $Au@TiO_2$ core-shell nanostructures, *Phys. Chem. Chem. Phys.*, in preparation

25. Ji Bong Joo, Qiao Zhang, Michael Dahl, Francisco Zaera, Yadong Yin, Synthesis, Crystallinity Control, and Photocatalysis of Nanostructured TiO_2 Shells, *J. Mater. Res.*, in preparation.

26. Francisco Zaera, Nanostructured Materials for Applications in Heterogeneous Catalysis, *Chem. Soc. Rev.*, in preparation. INVITED

27. Qiao Zhang, Ilkeun Lee, Ji Bong Joo, Francisco Zaera and Yadong Yin, Core-Shell Nanostructured Catalysts, *Acc. Chem. Res.*, in preparation. INVITED

28. Ji Bong Joo, Ilkeun Lee, Michael Dahl, Geondae Moon, Francisco Zaera, Yadong Yin, Controllable Synthesis of Mesoporous TiO_2 Hollow Shells: Toward an Efficient Photocatalyst, *Adv. Func. Mater.*, in preparation.

Papers Funded by other Federal or Non-Federal Sources.

1. On the Film Thickness Dependence of Shear Strengths in Sliding, Boundary-Layer Friction, Michael Garvey, Michael Weinert and Wilfred T. Tysoe, *Wear,* **274-275**, 281 (2012)

2. shear-Induced Boundary Film Formation from Dialkyl Sulfides on Copper, O. Furlong, B. Miller and W.T. Tysoe, *Wear,* **274-275,** 183 (2012)

3. The Adsorption of Acetic Acid on Clean and Oxygen-covered Au/Pd(100) Alloy Surfaces, Zhenjun Li and Wilfred T. Tysoe, *Surface Science,* **606**, 1934-1941 (2012)

4. The Structure of the Au/Pd(100) Alloy Surface, Michael Garvey, Jorge A. Boscoboinik, Luke Burkholder, Joshua Walker, Craig Plaisance, Matthew Neurock, and Wilfred T. Tysoe, *J. Phys. Chem. C.,* **116,** 4692-4697 (2012)

5. The Adsorption and Reaction of Vinyl Acetate on Au/Pd(100) Alloy Surfaces, Zhenjun Li, Florencia Calaza and Wilfred T. Tysoe, *Surface Science,* **606,** 1113-1119 (2012)

6. The Surface Chemistry of Isopropoxy Tetramethyl Dioxaborolane on Copper, Brendan P. Miller, Octavio J. Furlong, and Wilfred. T. Tysoe, *Langmuir* **28**, 6322 (2012)

7. Relating Molecular Structure to Tribological Chemistry: Borate Esters on Copper, Brendan P. Miller, Peter V. Kotvis, Octavio J. Furlong and Wilfred T. Tysoe, *Tribology Letters,* **49**, 21-29 (2012)

8. The Kinetics of Shear-Induced Boundary Film Formation from Dimethyl Disulfide on Copper, Brendan Miller, Octavio Furlong and Wilfred T. Tysoe, *Tribology Letters,* **49,** 39-46 (2102)

9. Linking Gold Nanoparticles with Conductive, 1,4 –Phenylene Diisocyanide–Gold Oligomers, John Kestell, Rasha Abuflaha, J. Anibal Boscoboinik, Yun Bai, Dennis W. Bennett and Wilfred T. Tysoe, *Chemical Communications,* in preparation

10. Pressure Dependence of the Shear Strengths of the Tungsten Carbide-Potassium Chloride Interface, Michael Garvey, Michael Weinert and Wilfred T. Tysoe, *Tribology Letters,* in preparation

11. Temperature and Velocity Dependences in the Tomlinson/Prandtl Model for Atomic Sliding Friction, Sergio Manzi, Wilfred T. Tysoe and Octavio Furlong, *Physical Review Letters,* submitted

12. Mechanistic Insights in the Catalytic Synthesis of Vinyl Acetate on Palladium and Gold/Palladium Alloy Surfaces, Matthew Neurock and Wilfred T. Tysoe, Topics in Catalysis, submitted

13. The Desorption and Reaction of 1-Alkenes and 1-Alkynes on Cu(111) and Copper Foils, Brendan P. Miller, Octavio J. Furlong and Wilfred T. Tysoe, *Surface Science*, submitted

14. Tribological Properties of 1-Alkenes on Copper Foils; Effect of Low-coordination Surface Sites, Brendan P. Miller, Octavio J Furlong and Wilfred T. Tysoe, *Tribology Letters,* submitted

15. B. Fleutot, J.B. Miller, A.J. Gellman, "Apparatus for deposition of composition spread alloy films: The rotatable shadow mask" *Journal of Vacuum Science and Technology – A*, **30(6),** (2012), 061511-1-10

16. A. de Alwis, B. Holsclaw, V.V. Pushkarev, A. Reinicker, T.J. Lawton, M.E. Blecher, E.C.H. Sykes, AJ. Gellman, "Surface structure spread single crystals (S^4C): Preparation and characterization" *Surface Science*, submitted

17. S.D. Miller, V.V. Pushkarev, A.J. Gellman, J.R. Kitchin, "Simulating temperature programmed desorption of oxygen on Pt(111) using DFT derived coverage dependent desorption barriers" *Topics in Catalysis*, submitted

18. T.J. Lawton, V. Pushkarev,D. Wei, F. Lucci, D. S. Sholl, A.J. Gellman, E.C.H. Sykes, "Long Range Chiral Restructuring of Cu(110) by Tartaric Acid" *Journal of Physical Chemistry C* submitted

19. Qing Zhao, Rongping Deng, and Francisco Zaera, Thermal Activation and Reaction of Allyl Alcohol on Ni(100), *Surf. Sci.*, **605(13/14)**, 1236-1242 (2011).

20. Min Shen, Hansheng Guo, Francisco Zaera, Bond Forming Reactions Involving C_1 Moieties: Late vs. Early Transition Metal Surfaces, *Top. Catal.*, **54(8)**, 482-489 (2011). INVITED (Special Issue, Mexican Congress of Catalysis)

21. Shermin Arab, Dongsheng Li, Nichola Kinsinger, Francisco Zaera, David Kisailus, Solvothermal Synthesis of a Highly Branched Ta-doped TiO_2, *J. Mater. Res.*, **26(20)** 2653-2659 (2011).

22. Yongfeng Zhao, Yan Liu, Ilkeun Lee, Yang Song, Xiangdong Qin, Francisco Zaera, Jiayu Liao, Chemoselective Fabrication of High Density Peptide Microarray by Hetero-bifunctional Tetra(ethylene glycol) Linker for Click Chemistry Conjugation, *J. Biomed. Mater. Res. A*, **100(1)**, 103-110 (2012).

23. Shirui Guo, Maziar Ghazinejad, Xiangdong Qin, Huaxing Sun, Wei Wang, Francisco Zaera, Cengiz S. Ozkan, Mihrimah Ozkan, Tuning of Electron Transport in Graphene based Field Effect Devices using Block Co-Polymers, *Small*, **8(7)**, 1073-1080 (2012).

24. Aashani Tillekaratne, Juan Pablo Simonovis, Maria Francisca Lopez, Maryam Ebrahimi, Francisco Zaera, Operando Studies of the Catalytic Hydrogenation of Ethylene on Pt(111) Single Crystal Surfaces, *ACS Catalysis*, **2(11)**, 2259–2268 (2012). INVITED

25. Francisco Zaera, Key Unanswered Questions About the Mechanism of Olefin Hydrogenation Catalysis by Transition-metal Surfaces, *Phys. Chem. Chem. Phys.*, submitted. INVITED, SPECIAL ISSUE: "Interfacial Phenomena in (De)hydrogenation Reactions."

26. Francisco Zaera, Kinetics on Model Systems, in *Comprehensive Inorganic Chemistry II*, Jan Reedijk and Ken Poeppelmeier, editors, Volume 7: Surface Inorganic Chemistry and Metal-Based Catalysis, Robert Schloegl, editor, Section 8, accepted. INVITED

27. Ilkeun Lee and Francisco Zaera, Shape Selectivity in Catalysis: Butene Isomerization and Hydrogenation on Platinum, *Top. Catal.*, in press. INVITED, SPECIAL ISSUE: "in Memory of D. W. Goodman."